Early-mid Miocene erosion rates measured in pre-Dead Sea rift Hazeva River using cosmogenic ^{21}Ne in fluvial chert pebbles

Michal Ben-Israel[1], Ari Matmon[1], Alan J. Hidy[2], Yoav Avni[3], Greg Balco[4]

[1]*The Institute of Earth Sciences, Hebrew University of Jerusalem, Jerusalem, 91904, Israel*

5   [2]*Center for Accelerator Mass Spectrometry, Lawrence Livermore National Laboratory, Livermore, CA 94550, USA*

[3]*Geological Survey of Israel, Yesha'yahu Leibowitz 32, Jerusalem, 96921 Israel*

[4]*Berkeley Geochronology Center, Berkeley, California 94709, USA*

Correspondence to: Michal Ben-Israel (michal.benisrael@mail.huji.ac.il)

Abstract. The Miocene Hazeva River was a large fluvial system (estimated catchment size

10   >100,000 km²) that drained the Arabian Plateau and Sinai Peninsula into the Mediterranean Sea during the Early-Mid Miocene. It was established after rifting of the Red Sea uplifted the Arabian Plateau during the Oligocene. Following late Miocene to early Pliocene subsidence along the Dead Sea Rift, the Hazeva drainage system was abandoned and dissected, resulting in new drainage divides on either side of the rift. We utilized a novel application of cosmogenic ^{21}Ne measurements

15   in chert to compare modern erosion rates with Miocene erosion rates that operated when the Hazeva River was active. We find that modern erosion rates derived from cosmogenic ^{21}Ne, ^{26}Al, and ^{10}Be in exposed *in situ* chert nodules to be extremely slow, between 2-4 mm/kyr. Comparison between modern and paleo erosion rates, measured in chert pebbles, is not straightforward, as cosmogenic ^{21}Ne was acquired partly during bedrock exhumation and partly during transport of

20   these pebbles in the Hazeva River. However, even with bedrock erosion and maintained transport along this big river, ^{21}Ne concentrations measured in Miocene cherts are lower (range between 3.66±1.9x10⁶ and 8.97±1.39x10⁶ atoms/g SiO₂) compared to ^{21}Ne concentrations measured in the currently eroding chert nodules (8.08±1.48x10⁶ and 12.10±2.43x10⁶ atoms/g SiO₂). ^{21}Ne concentrations in Miocene cherts correspond to minimum erosion rates that are at least twice as

25 fast as rates calculated today. We attribute these faster erosion rates to a combination of continuous

uplift and significantly wetter climatic conditions during the Miocene.

1. Introduction

Tectonic and climatic conditions control geomorphological processes through surface uplift, rock weathering, and sediment generation and transport (e.g., Allen, 2008; Whipple, 2009; Whittaker,

30 2012). Fluvial systems and their associated sediment archives respond to and record changes in rates of continental uplift and climatic conditions as rates of erosion influence sediment production, transport, and storage (e.g., DiBiase and Whipple, 2011; Ferrier et al., 2013; Vance et al., 2003). Cosmogenic nuclides have long been applied to quantify such rates in diverse geological settings (e.g., Bierman, 1994; von Blanckenburg, 2005). However, the further back in time we go,

35 the less information there is about rates of surface shaping processes. This is mostly due to decreasing preservation potential of older landscapes, as active surface processes destroy evidence of transient landscapes. Furthermore, even when geological circumstances do allow for the preservation of slowly eroding surfaces, erosion rates prior to the Pliocene cannot be quantified with the more commonly used cosmogenic radionuclides (^{10}Be and ^{26}Al) due to their half-lives

40 (1.38 Myr and 716 kyr, accordingly; Ivy-Ochs and Kober, 2008). Stable cosmogenic nuclides have the potential to quantify rates of surface processes significantly older than commonly used cosmogenic radionuclides (Balco et al., 2019; Ben-Israel et al., 2018; Dunai et al., 2005; Libarkin et al., 2002; Sinclair et al., 2019). Here, we apply stable cosmogenic ^{21}Ne to sediments deposited during the early-mid Miocene by a massive fluvial system that drained parts the Arabian Peninsula

45 and Sinai into the Mediterranean prior to the subsidence of the Arava Valley along the Dead Sea transform (Garfunkel and Horowitz, 1966; Zilberman and Calvo, 2013). The rates of surface processes deduced from Miocene river sediments open a window into the tectonic and climatic regimes that dominated the region during this time.

2. Geological Background

50 The tectonic and magmatic events leading to the rifting of the Red Sea and the Gulf of Aden and the emergence of the Afar plume during the Oligocene (~35-30 Ma) triggered regional uplift (e.g., Bohannon et al., 1989; Bosworth et al., 2005; Omar and Steckler, 1995). During the last 20-30 Myr, the Arabian Peninsula has been uplifting from near sea level to its present elevation of ~1km

(Bar et al., 2016; Wilson et al., 2014). As a result of widespread erosion following this uplift, a
regional truncation surface developed in the northern Red Sea and the southern Levant and exposed
older strata down to Precambrian formations depending on the preexisting structure (Avni et al.,
2012). During the Miocene, the uplifted region was drained by a newly established fluvial system,
termed the Hazeva River, which flowed northwestward from the uplifted terrains towards the
Mediterranean Sea, and drained an estimated area >100,000 km^2 (Garfunkel and Horowitz, 1966;
Zilberman and Calvo, 2013; Fig. 1).

At present, the mostly clastic sedimentary sequence deposited by this fluvial system is preserved
mainly in structural lows, karstic systems, and abandoned stream valleys in southern Israel, eastern
Sinai, and Jordan (Calvo and Bartov, 2001; Fig. 2). The sediments associated with this Miocene
fluvial system compose the Hazeva formation in southern Israel. This formation is divided into
two major parts, the lower includes autochthonous conglomerates and lacustrine carbonate units,
and the upper part is comprised of allochthonous clastic units, mainly quartz sand and chert pebbles
(Calvo, 2002). Here we focus on the allochthonous silicate sediments of the upper part. The onset
of the Hazeva River is constrained by the Karak dike (~20 Myr) which intrudes the lower section
of the Hazeva formation (Calvo and Bartov, 2001). The Hazeva fluvial system operated until the
subsidence of the Dead Sea Rift during the late Miocene to early Pliocene brought on a dramatic
change in morphology, which led to the dismantlement of this massive fluvial system, the last of
its kind in the region (Garfunkel, 1981). By the early Pliocene, the Hazeva River was abandoned,
and new independent drainage systems drained the region toward the Dead Sea Basin (Avni et al.,
2001).

3. Methodology and Analytical Procedures

3.1 Sampling Strategy

Cosmogenic nuclides in sediments accumulate throughout the sedimentary cycle as near-surface
material is exposed during weathering and exhumation of the source rock, during transport in a
specific drainage system, and to a much lesser degree following burial at some intermediate or
final destination. Unlike the more commonly used radioactive cosmogenic nuclides, which may
decay substantially or even completely over multiple cycles, ^{21}Ne is stable. This means that the
concentration of ^{21}Ne measured in the sediment may have accumulated over several sedimentary
cycles, i.e., after the sediment reaches the depositional basin, sediment can be re-exhumed and

once again exposed and transported in a new sedimentary cycle. Therefore, the concentration of

85 cosmogenic ^{21}Ne measured in sediment represents total exposure during previous and current sedimentary cycles. This should hold true so long as intermittent burial does not expose the sediment to temperatures exceeding the geological closure temperature of Ne in quartz (90-100°C; Shuster and Farley, 2005), corresponding to ~2-3 km burial depth given a geothermal gradient of 30-50°C/km.

90 The upper part of the Hazeva formation contains a clastic sequence composed of two different silicate members that were exposed, eroded, and deposited at the same time. The first is sub-rounded monocrystalline quartz-arenite, eroded from Phanerozoic Nubian sandstone as well as from outcrops of Precambrian crystalline rocks of the Arabian-Nubian shield (Calvo and Bartov, 2001). The second member consists of well-rounded chert pebbles either interbedded with the

95 quartz sand or forming horizons of pebbles in the sandy sequence (Zilberman and Calvo, 2013). The chert composing these pebbles is sourced only from east of the Dead Sea Rift, and therefore fluvial deposits on the west side containing this "imported chert" (Kolodny, 1965) must have been emplaced prior to rifting. The quartz sand and the chert pebbles were both transported by the Miocene Hazeva system and share an overall similar exposure history. However, the quartz sand

100 was exposed in previous sedimentary cycles throughout the Mesozoic and Paleozoic where it accumulated cosmogenic ^{21}Ne. In contrast, the chert was deposited in the Eocene and then exposed, transported, and buried during the Miocene (Avni et al., 2012). Therefore, while the cosmogenic ^{21}Ne measured in the quartz sand represents multiple sedimentary cycles, the cosmogenic ^{21}Ne measured in the chert pebbles represents erosion and transport during a single

105 sedimentary cycle in the Miocene Hazeva River.

We collected and analyzed ten samples in total. Three samples of quartz sand (MHS1, MHS3, and MHS5) and five individual chert pebbles (MHC2, MHC23, MHC5a MHC2b, and MHC6) were obtained from two Miocene Hazeva deposits (Fig. 2 B-C; Table 1). At both sites, samples were collected from deeply shielded locations to minimize the effects of post-burial production. Two

110 individual samples of *in situ* chert nodules (EJC3 and EJC5) were collected from exposed bedrock outcrops of the Eocene source rock in central Jordan (Fig. 2 A). Unlike the Miocene samples, which were exposed during at least one full sedimentary cycle, the modern chert nodules accumulated cosmogenic nuclides during exhumation to the modern surface. These concentrations thus represent averaged rates of surface denudation over the ~10^5 yr time-scales.

3.2 Preparation of Chert and Quartz Samples and Analytical Procedures

Chert and quartz samples were processed to separate clean SiO_2 at the Institute of Earth Sciences Cosmogenic Isotope Laboratory, Hebrew University of Jerusalem, following standard procedures (Hetzel et al., 2002; Kohl and Nishiizumi, 1992). The samples were first leached in HCl/HNO_3 mixture (3:1) at a temperature of 150°C for 1.5h dissolving carbonates and iron oxides. This procedure was followed by Franz magnetic separation to remove magnetic grains, including quartz grains that contain inclusions of magnetic material. Samples were then leached three times in a 1% HF/HNO_3 mixture for 7, 12 and 24h at 70°C, removing the outer rims of the quartz grains. Aliquots of all 10 etched samples were then analyzed for Ne isotopes at the Berkeley Geochronology Center. Chert samples were washed with isopropanol to remove fine chert particles attached to the chert grains. Aliquots from samples MCH5A and EJC5 were crushed to compare the degassing results with the uncrushed aliquots. Ca. 70 mg from the chert samples and ca. 150 mg from the quartz samples were encapsulated in a tantalum packet and heated under vacuum using a diode laser micro-furnace at 2-4 heating steps between 450 and 1250°C for 15 minutes at each temperature step. Ne isotope measurements used the BGC "Ohio" system and the procedure described in Balco et al., (2019). 20-30 grams of leached and clean quartz from three quartz samples and three chert samples were processed to separate Be and Al oxides following Kohl and Nishiizumi (1992) and Bierman and Caffee (2001). These were then analyzed for $^{10}Be/^9Be$ and $^{26}Al/^{27}Al$ at the Centre for Accelerator Mass Spectrometry, Lawrence Livermore National Laboratory and calibrated against house standards and blanks.

4. Results

4.1 ^{21}Ne in Quartz Sand and Cherts

For the chert samples, <2% of the total ^{21}Ne and no more than 1% of the total ^{20}Ne measured were released above 950°C (see the Supplementary Tables S1-4), therefore subsequent analyses were performed at 450, 700, and 950°C heating steps for chert samples and 950 and 1250°C heating steps for quartz samples (Table 1). Of the total ^{21}Ne measured, >85% was released at the low-temperature steps, below the 950°C step in the chert samples and below the 1250°C step in the quartz samples (see Supplementary Tables S1-4). Also, low-temperature $^{21}Ne/^{20}Ne$ and $^{22}Ne/^{20}Ne$ ratios fall on the spallation line, within analytical uncertainty. Therefore, we conclude that excess ^{21}Ne relative to an atmospheric isotopic $^{21}Ne/^{20}Ne$ ratio of 0.002959 ($^{21}Ne_{ex}$) in the low-

145 temperature steps is a good representation for cosmogenic ^{21}Ne (^{21}Ne$_{cos}$; see Supplementary Fig. S8-12). While most samples show some increase in the low-temperature ^{21}Ne$_{ex}$, sample MHC2 shows no enrichment in ^{21}Ne/^{20}Ne ratio and very little enrichment in ^{22}Ne/^{20}Ne ratio compared to atmospheric composition in the low-temperature steps. In the 950°C step, there is enrichment compared to atmospheric values. However, as only ~12% of the total ^{21}Ne was released in the

150 950°C step, determining the concentration of cosmogenic ^{21}Ne in sample MHC2 is beyond analytical abilities. Therefore, this sample was not considered in further calculations, discussion, and interpretations. It is important to note that even with cosmogenic isotopic values of ^{21}Ne/^{20}Ne and ^{22}Ne/^{20}Ne ratios at the low-temperature steps, distinguishing the cosmogenic component of ^{21}Ne$_{ex}$ from the nucleogenic component, produced by the decay of U and Th within the crystal

155 lattice, is not trivial. Nonetheless, as all chert samples (Eocene chert nodules and Miocene chert pebbles) share the same lithology, any differences in the ^{21}Ne$_{ex}$ concentrations must be due to the cosmogenic component.

The chert pebbles and quartz sands sampled at both Miocene Hazeva sites show variable concentrations of ^{21}Ne$_{cos}$ ranging between $0.00 \pm 1.88 \cdot 10^6$ and $8.89 \pm 1.83 \cdot 10^6$ atoms/g SiO$_2$ (Fig. 3).

160 At both Miocene Hazeva sites, the cosmogenic ^{21}Ne concentrations measured in chert pebbles are similar or lower compared to sand samples. These measured concentrations agree with our understanding that the sand samples contain quartz grains that originated from various sandy units that were deposited throughout the Phanerozoic and could have undergone several sedimentary cycles before they were exhumed and transported by the Miocene fluvial system. Alternatively,

165 the sand samples could have higher concentrations of nucleogenic ^{21}Ne as the source rock for this sand is >800 Ma (Kolodner et al., 2009). Conversely, the chert samples are derived from a relatively young, Eocene, source rock, and only participated in one sedimentary cycle during the Miocene. The chert nodule samples collected from *in situ* Eocene outcrops show higher cosmogenic ^{21}Ne concentrations compared to the Miocene chert pebbles (Fig 3).

170 **4.2 ^{10}Be and ^{26}Al in Quartz Sand and Cherts**

^{10}Be and ^{26}Al concentrations were measured in three Miocene sand samples (MHS1, MHS3, and MHS5), the two Eocene chert nodules (EJC3 and EJC5) and two chert pebbles (MHC5b and MHC6). ^{10}Be results for sample MHC5b and ^{26}Al results for sample MHS1 are not available (Table 1). Miocene sand and chert samples show ^{10}Be and ^{26}Al that are low and consistent with extended

175 periods of burial ($\leq 0.39 \pm 0.03 \cdot 10^5$ atoms/g SiO$_2$ for ^{10}Be and $\leq 4.33 \pm 0.55 \cdot 10^5$ atoms/g SiO$_2$ for

[26]Al). Currently eroding Eocene nodules show higher concentrations of [10]Be and [26]Al with sample EJC3 showing [26]Al/[10]Be ratio that is consistent with production at the surface, and sample EJC5 showing a lower [26]Al/[10]Be ratio, suggesting a more complicated exposure history (see Discussion section).

180 ## 5. DISCUSSION

5.1 Correcting for Post-Burial Muonic Produced Cosmogenic [21]Ne

When examining concentrations of cosmogenic nuclides in sediments that have been buried for extended periods, post-burial production needs to be considered. At or near the surface, spallation interactions are the main pathway for *in situ* production of cosmogenic nuclides accounting for

185 >95% for [26]Al, [10]Be, and [21]Ne (Dunai, 2010). However, the relative contribution of production by muon interactions increases with burial depth, and while production rates are relatively low, they can be significant when integrated over long periods of time—especially for stable nuclides. The post-burial component does not represent surface processes, and therefore, it is crucial to account for its contribution to the measured cosmogenic component. For radioactive cosmogenic nuclides,

190 such as [10]Be and [26]Al, their initial concentrations (acquired during exposure) decrease post burial due to radioactive decay, with [26]Al decreasing faster than [10]Be according to their corresponding half-lives (e.g., Balco and Rovey, 2008; Granger, 2006; Granger and Muzikar, 2001; Lal, 1991). We calculated the expected concentrations of cosmogenic [26]Al, [10]Be, and [21]Ne in sediments over a burial period of 18 Myr, the likely age of the fluvial system stabilization (Bar and Zilberman,

195 2016). We then compared these calculated concentrations to the measured concentrations of [26]Al, [10]Be, and [21]Ne$_{cos}$ in Miocene chert and sand samples (Fig. 4). Both [10]Be and [26]Al measurements are only available for two buried sand samples, one buried chert pebble, and two *in situ* chert nodules (Table 1). The measured [10]Be and [26]Al concentrations have reached equilibrium that is consistent with an extended period of burial at depths between 20-120 m (given that overburden

200 consists of clastic sediments with a density of ~2 g/cm³). The discrepancy between the current burial depth, only tens of meters below the surface, and the deduced burial depth is likely the result of surface erosion that occurred during the last ~2 Myr (Matmon and Zilberman, 2017 and references therein). Additionally, the relatively large uncertainty on muogenic production rates could account for some of this discrepancy (Balco, 2017; Balco et al., 2019). The cosmogenic [21]Ne

205 produced post-burial over 18 Ma of burial at depths between 20-120 m is lower than measured for

the presented samples, accounting for a maximum of ~$1.3\cdot10^6$ atoms/g SiO_2. This concentration is lower than the analytical uncertainty for all measured Miocene samples except for MHC2, where no cosmogenic ^{21}Ne was measured. However, sample MHC2 is not considered in the interpretations of the results.

5.2 Calculating Modern and Miocene Rates of Surface Processes

Erosion rates calculated from cosmogenic ^{21}Ne concentrations measured in modern *in situ* chert nodules from the Jordanian Central Plateau (EJC3 and EJC5) range between 2-3 mm/kyr. Erosion rates calculated from ^{10}Be and ^{26}Al concentration measured in sample EJC5 are similar, 2-4 mm/kyr, with production rates scaled for latitude and altitude after Stone (2000), using production rates of 2.62 and 30.26 atoms/g SiO_2 year for ^{10}Be and ^{26}Al, respectively. In contrast, erosion rates calculated from ^{10}Be and ^{26}Al concentrations measured in sample EJC3 are 40-50 mm/kyr, an order of magnitude faster. While we cannot explain this discrepancy, we believe that the representative results are the slower erosion rates. Firstly, the ^{21}Ne calculated erosion rates in sample EJC3 (~2 mm/kyr) agrees with the ^{21}Ne, ^{26}Al, and ^{10}Be calculated erosion rates for sample EJC5. Secondly, modern erosion rates measured in chert bedrock in other hyperarid regions of eastern Mediterranean area also indicate rates of erosion that range between 1-5 mm/kyr (Boroda et al., 2013; Matmon et al., 2009; Matmon and Zilberman, 2016). We conclude that ^{21}Ne concentrations in modern Jordanian Central Plateau chert nodules indicate simple exposure times that range between 269±49 and 378±76 kyr, and equivalent erosion rates that range between 2-4 mm/kyr. It is important to note that modern calculated exposure times and erosion rates in the Jordanian cherts represent exhumation only.

Quantifying rates of surface processes that occurred during the Miocene using cosmogenic ^{21}Ne concentrations is not trivial, most notably due to the challenge in evaluating the local isotope production rates. As the latitude of the Arabian Peninsula during the early Miocene was similar to today (Meulenkamp and Sissingh, 2003 and references therein), the observed differences in cosmogenic ^{21}Ne concentrations between Miocene and modern chert samples can be equally explained by doubling the erosion rates during the Miocene or a 1 km difference in source elevation. It is not possible to determine with certainty what the elevation of the Jordanian Central Plateau was during the Miocene. However, the Arabian Peninsula was mostly submerged below sea level from the Late Cretaceous to the early Oligocene when uplift and exhumation began with the rifting of the Red Sea (Bohannon et al., 1989; Kohn and Eyal, 1981; Omar and Steckler, 1995).

Recent studies show that uplift and exhumation commenced 21-25 Ma and decreased significantly at ~18 Ma, reaching maximal elevations of ~2.5 km along the flanks of the Suez Rift (e.g., Bar et al., 2016; Morag et al., 2019). Still, the rate and history of uplift of the Arabian Peninsula are not

240 as well constrained. Recently, Wilson et al. (2014) proposed that the western half of the Arabian Peninsula experienced significant regional uplift during the last 25-30 Ma at rates of up to 0.1 mm/yr with topography initially forming in Yemen and slowly migrating northward. At present, the mean elevation of the Jordanian Central Plateau is ~1 km (Fig. 2). Taking into consideration the reported rates and timing of uplift it is reasonable to presume that the western flank of the

245 Arabian Peninsula reached its current elevation before the initiation of the Miocene Hazeva fluvial system at ~18 Ma. Furthermore, during the early Miocene, broad valleys (500-1000 m wide and ~100 m deep) incised the regional truncation surface that developed in the region during the Oligocene (Avni et al., 2012). The incision of these valleys, where the Hazeva formation was later deposited, suggests that significant uplift occurred prior to the deposition of fluvial sediments by

250 the Hazeva River. Therefore, we assume an elevation of 1km and latitude of 20-30° when for Miocene production rates, when calculating exposure times and erosion rates. The calculated exposure times of sediments in the Miocene Hazeva fluvial system are variable, and range between 63^{+0}_{-63} and 179±63 kyr (Fig. 3). As previously mentioned, the measured cosmogenic ^{21}Ne in the Miocene chert pebbles represents the total time of exposure during exhumation from bedrock

255 coupled with transport in the Hazeva River. The calculated exposure times are equivalent to minimal erosion rates of ~4-12 mm/kyr, at least twice as fast than those occurring today. Thus, the actual bedrock erosion rates during the Miocene would have been significantly faster than modern rates mentioned above.

5.3 Climatic and Tectonic Controls on Miocene Erosion Rates

260 The increased erosion rates, compared to modern, inferred from Miocene chert pebbles are the consequence of the environmental conditions that prevailed at that time. An increase in rates of surface erosion is most commonly attributed to perturbations in fluvial basins in response to tectonic uplift and/or warmer/wetter climatic conditions (e.g., DiBiase and Whipple, 2011; Romans et al., 2016; Schaller and Ehlers, 2006; Val et al., 2016; Willenbring et al., 2013). For

265 example, increased precipitation brings about higher river discharge and enhancement of the stream power available for bedrock erosion and sediment transport. Erosion rates in fluvial systems

also respond to tectonically induced changes in base level that increase slope steepness and instability, resulting in higher stream power and more sediment readily available for transport. Here we examine evidence from previous studies of the climatic and tectonic conditions that

270 prevailed in the region during the Miocene, capable of forcing the deduced rapid erosion rates. However, when examining ancient erosion rates, we must first consider the time-scales over which cosmogenic nuclides are averaged. The question arises whether the reported erosion rates accurately represent the environmental conditions of a certain period (e.g. the early to mid-Miocene) or if the calculated rates are the result of episodic oscillation or catastrophic geomorphic

275 events. For the modern erosion rates reported here, it is a reasonably simple answer. The modern erosion rates are relatively slow and so they integrate hundreds of thousands of years over which such oscillations or rare catastrophic events would be averaged. As for the Miocene erosion rates, samples were collected from two separate sites and from different depths, so it is unlikely that they all represent the exception. We, therefore, consider the range of rates obtained from Miocene

280 samples to be a good representation for Miocene surface processes.

Many works which quantify the rates and timing of uplift related to the rifting of the Red Sea are confined to the edges of the Arabian plate and do not give good constrains for intercontinental uplift (Bar et al., 2016; Morag et al., 2019; Omar et al., 1989; Omar and Steckler, 1995). Collectively, these studies show a decrease in exhumation rates during the mid-Miocene (~18

285 Myr). While uplift rates decreased during the Miocene, tectonic uplift and topographic changes could still drive large-scale landscape response, manifesting as increased erosion rates and the establishment of the Hazeva fluvial system.

In addition to tectonic forcing, there is ample evidence for a warmer and wetter climate in the region during the Miocene. Locally, the appearance of mammals in the Negev along with arboreal

290 and grassy vegetation during the early-mid Miocene supports a humid environment (Goldsmith et al., 1988; Horowitz, 2002; Tchernov et al., 1987). Tropical to subtropical climate prevailed in the eastern Arabian Peninsula, as indicated by fossilized mangrove roots (Whybrow and McClure, 1980). Locally, Kolodny et al. (2009), interpreted the ^{18}O in lacustrine limestone from the lower part of the Hazeva unit to be deposited by ^{18}O-depleted paleo-meteoric water. They proposed that

295 the presence of a warm ocean to the southeast of the region during the Late Oligocene-Early Miocene resulted in tropical cyclones being more prevalent and increasing rainfall in the region.

Together, the above observations suggest climatic conditions that could promote erosion rates which are faster than those observed in hyperarid conditions (such as prevail today) and could also support and maintain the existence of a great fluvial system, such as the Hazeva River, during the

300 Miocene.

6. Conclusions

We compared the cosmogenic ^{21}Ne measured in chert pebbles and quartz sand eroded and transported during the mid-Miocene (~18 Myr) by the Hazeva River with the chert source rock (Eocene chert nodules) currently eroding in the Central Jordanian Plateau.

305 We successfully established a novel application for measuring cosmogenic ^{21}Ne in modern and Miocene chert samples, expanding the opportunities and settings in which stable cosmogenic nuclides analysis could be used as a tool to quantify geomorphic processes and ascertaining chert as a viable lithologic target for cosmogenic Ne analysis. In modern samples, measurements of cosmogenic nuclides ^{10}Be and ^{26}Al generally agree with ^{21}Ne results. In the Miocene samples,

310 cosmogenic ^{21}Ne in quartz sand samples is equal or higher compared to Miocene chert pebbles, agreeing with the geologic understanding that sand has experienced several sedimentary cycles where ^{21}Ne was produced, while chert experienced only one such cycle in the Miocene Hazeva fluvial system.

Exposure times calculated from the measured cosmogenic ^{21}Ne concentrations in the Miocene

315 chert pebbles are considerably shorter compared to the chert nodules currently eroding in the Central Jordanian Plateau. While, it is impossible to determine the exact rate of erosion during the Miocene as cosmogenic ^{21}Ne was produced both during erosion from the bedrock and transport in the river, the shorter exposure times during the Miocene reflect faster rates of surface processes that correlate to minimal erosion rates that are at least twice as fast. The cause for increased rates

320 of surface processes during the Miocene cannot be easily constrained to either tectonic or climatic conditions. The entire region experienced tectonic uplift and exhumation that while decreasing during the Mid-Miocene brought on topographic changes that established the Hazeva fluvial system and could have been manifested as faster rates of surface erosion. Furthermore, multiple independent proxies presented in previous studies support wetter climatic conditions in the region

325 during the early-mid Miocene. Increased precipitation would explain the faster rates of bedrock erosion deduced as well as the higher water discharge needed to maintain transport along the

Hazeva River. While it is possible that rates of erosion or it changed significantly throughout the Miocene, the variability in ^{21}Ne concentrations measured in Miocene chert samples are more likely the result of fluvial transport dynamics, temporary storage, and exposure during transport in this

330 large Miocene river.

Data availability

A raw data table including all Ne isotope measurements and three-isotope plots are available in supplement.

Author contribution

335 MBI and AM designed the study. MBI collected the samples for analysis with assistance from AM and YA. MBI prepared samples for analyses and measured ^{21}Ne/^{20}Ne and ^{22}Ne/^{20}Ne ratios with GB, and AJH measured the ^{10}Be/^{9}Be and ^{26}Al/^{27}Al ratios. MBI analyzed the data, produced the figures, and prepared the manuscript with contributions from all co-authors.

Competing interests

340 The authors declare that they have no conflict of interest.

Acknowledgments

This work was funded by the Israel Science Foundation (*ISF* grant number 385/14 to AM) and further supported by the United States-Israel Binational Science Foundation (BSF travel grant T-2017229 to MBI). Our gratitude to Y. Geller, O. Tirosh, and Y. Burstyn for laboratory and field
345 assistance. MBI would like to thank the technical and administrative staff at the Berkeley Geochronology Center for their assistance and support. This work was performed in part under the auspices of the U.S. Department of Energy by Lawrence Livermore National Laboratory, United States under Contract DE-AC52-07NA27344. This is LLNL-JRNL-788357.

References

350 Allen, P. A.: From landscapes into geological history, Nature, 451(7176), 274–276,

doi:10.1038/nature06586, 2008.

Avni, Y., Bartov, Y., Ginat, H. and Ginata, H.: The Arava Formation-A Pliocene sequence in the Arava Valley and its western margin, southern Israel, Isr. J. Earth Sci., 50(2), 101–120, doi:10.1092/5U6A-RM5E-M8E3-QXM7, 2001.

355 Avni, Y., Segev, A. and Ginat, H.: Oligocene regional denudation of the northern Afar dome: Pre- and syn-breakup stages of the Afro-Arabian plate, Bull. Geol. Soc. Am., 124(11–12), 1871–1897, doi:10.1130/B30634.1, 2012.

Balco, G.: Production rate calculations for cosmic-ray-muon-produced [10]Be and [26]Al benchmarked against geological calibration data, Quat. Geochronol., 39, 150–173,

360 doi:10.1016/j.quageo.2017.02.001, 2017.

Balco, G. and Rovey, C. W.: An isochron method for cosmogenic-nuclide dating of buried soils and sediments, Am. J. Sci., 308(10), 1083–1114, doi:10.2475/10.2008.02, 2008.

Balco, G., Blard, P.-H., Shuster, D. L., Stone, J. O. H. and Zimmermann, L.: Cosmogenic and nucleogenic [21]Ne in quartz in a 28-meter sandstone core from the McMurdo Dry Valleys,

365 Antarctica, Quat. Geochronol., 52, 63–76, doi:10.1016/j.quageo.2019.02.006, 2019.

Bar, O. and Zilberman, E.: Subsidence and conversion of the Dead Sea basin to an inland erosion base level in the early middle Miocene as inferred from geomorphological analysis of its ancient western fluvial outlet, Geomorphology, 261, 147–161, doi:10.1016/j.geomorph.2016.02.028, 2016.

370 Bar, O., Zilberman, E., Feinstein, S., Calvo, R. and Gvirtzman, Z.: The uplift history of the Arabian Plateau as inferred from geomorphologic analysis of its northwestern edge, Tectonophysics, 671, 9–23, doi:10.1016/j.tecto.2016.01.004, 2016.

Ben-Israel, M., Matmon, A., Haviv, I. and Niedermann, S.: Applying stable cosmogenic [21]Ne to understand surface processes in deep geological time (10^7–10^8 yr), Earth Planet. Sci. Lett., 498,

375 266–274, doi:10.1016/j.epsl.2018.07.002, 2018.

Bierman, P. R.: Using in situ produced cosmogenic isotopes to estimate rates of landscape evolution: A review from the geomorphic perspective, J. Geophys. Res., 99(B7), 13885–13896, doi:10.1029/94JB00459, 1994.

Bierman, P. R. and Caffee, M.: Slow Rates of Rock Surface Erosion and Sediment Production

380 across the Namib Desert and Escarpment, Southern Africa, Am. J. Sci., 301(4–5), 326–358, doi:10.2475/ajs.301.4-5.326, 2001.

von Blanckenburg, F.: The control mechanisms of erosion and weathering at basin scale from cosmogenic nuclides in river sediment, Earth Planet. Sci. Lett., 237(3–4), 462–479, doi:10.1016/j.epsl.2005.06.030, 2005.

385   Bohannon, R. G., Naeser, C. W., Schmidt, D. L. and Zimmermann, R. A.: The timing of uplift, volcanism, and rifting peripheral to the Red Sea: A case for passive rifting?, J. Geophys. Res., 94(B2), 1683, doi:10.1029/JB094iB02p01683, 1989.

Borchers, B., Marrero, S., Balco, G., Caffee, M., Goehring, B., Lifton, N., Nishiizumi, K., Phillips, F., Schaefer, J. and Stone, J.: Geological calibration of spallation production rates in the

390   CRONUS-Earth project, Quat. Geochronol., 31, 188–198, doi:10.1016/j.quageo.2015.01.009, 2016.

Boroda, R., Matmon, A., Amit, R., Haviv, I., Porat, N., Rood, D., Eyal, Y. and Enzel, Y.: Long-term talus flatirons formation in the hyperarid northeastern Negev, Israel, Quat. Res., 79(2), 256–267, doi:10.1016/j.yqres.2012.11.012, 2013.

395   Bosworth, W., Huchon, P. and McClay, K.: The Red Sea and Gulf of Aden Basins, J. African Earth Sci., 43(1–3), 334–378, doi:10.1016/j.jafrearsci.2005.07.020, 2005.

Calvo, R.: Stratigraphy and petrology of the Hazeva Formation in the Arava and the Negev: Implications for the development of sedimentary basins and the morphotectonics of the Dead Sea Rift Valley, Geol. Surv. Isr. Rep., GSI/22/02, 1–264, doi:GSI/22/02, 2002.

400   Calvo, R. and Bartov, Y.: Hazeva Group , southern Israel : New observations , and their implications for its stratigraphy , paleogeography , and tectono-, Isr. J. Earth Sci., 50(April), 71–99, doi:10.1560/B02L-6K04-UFQL-KUE3, 2001.

DiBiase, R. A. and Whipple, K. X.: The influence of erosion thresholds and runoff variability on the relationships among topography, climate, and erosion rate, J. Geophys. Res., 116(F4),

405   F04036, doi:10.1029/2011JF002095, 2011.

Dunai, T. J.: Cosmogenic Nuclides: Principles, Concepts and Applications in the Earth Surface Sciences, edited by Intergovernmental Panel on Climate Change, Cambridge University Press, Cambridge., 2010.

Dunai, T. J., González López, G. a. and Juez-Larré, J.: Oligocene-Miocene age of aridity in the

410   Atacama Desert revealed by exposure dating of erosion-sensitive landforms, Geology, 33(4), 321–324, doi:10.1130/G21184.1, 2005.

Ferrier, K. L., Huppert, K. L. and Perron, J. T.: Climatic control of bedrock river incision,

Nature, 496(7444), 206–209, doi:10.1038/nature11982, 2013.

Garfunkel, Z.: Internal structure of the Dead Sea leaky transform (rift) in relation to plate

415   kinematics, Tectonophysics, 80, 81–108, doi:10.1016/0040-1951(81)90143-8, 1981.

Garfunkel, Z. and Horowitz, A.: The upper Tertiary and Quaternary morphology of the Negev,

Israel, Isr. J. Earth Sci., 15(3), 101–117, 1966.

Goldsmith, N. F., Hirsch, F., Friedman, G. M., Tchernov, E., Derin, B., Gerry, E., Horowitz, A.

and Weinberger, G.: Rotem mammals and Yeroham crassostreids: stratigraphy of the Hazeva

420   Formation (Israel) and the paleogeography of Miocene Africa, Newsletters Stratigr., 20(2), 73–

90, 1988.

Granger, D. E.: A review of burial dating methods using ^{26}Al and ^{10}Be, in Special Paper 415: In

Situ-Produced Cosmogenic Nuclides and Quantification of Geological Processes, vol. 415,

edited by A. M. Alonso-Zarza and L. H. Tanner, pp. 1–16, Geological Society of America.,

425   2006.

Granger, D. E. and Muzikar, P. F.: Dating sediment burial with in situ-produced cosmogenic

nuclides: theory, techniques, and limitations, Earth Planet. Sci. Lett., 188(1–2), 269–281,

doi:10.1016/S0012-821X(01)00309-0, 2001.

Hetzel, R., Niedermann, S., Ivy-Ochs, S., Kubik, P. W., Tao, M. and Gao, B.: ^{21}Ne versus ^{10}Be

430   and ^{26}Al exposure ages of fluvial terraces: the influence of crustal Ne in quartz, Earth Planet. Sci.

Lett., 201(3–4), 575–591, doi:10.1016/S0012-821X(02)00748-3, 2002.

Horowitz, A.: Elephants, horses, humans, and others: Paleoenvironments of the Levantine land

bridge, Isr. J. Earth Sci., 51(3–4), 203–209, doi:10.1560/YTDR-LW6B-VHR7-69PY, 2002.

Ivy-Ochs, S. and Kober, F.: Surface exposure dating with cosmogenic nuclides, Quat. Sci. J., 57,

435   179–209, doi:10.3285/eg.57.1-2.7, 2008.

Kohl, C. P. and Nishiizumi, K.: Chemical isolation of quartz for measurement of in-situ -

produced cosmogenic nuclides, Geochim. Cosmochim. Acta, 56(9), 3583–3587,

doi:10.1016/0016-7037(92)90401-4, 1992.

Kohn, B. P. and Eyal, M.: History of uplift of the crystalline basement of Sinai and its relation to

440   opening of the Red Sea as revealed by fission track dating of apatites, Earth Planet. Sci. Lett.,

52(1), 129–141, doi:10.1016/0012-821X(81)90215-6, 1981.

Kolodner, K., Avigad, D., Ireland, T. R. and Garfunkel, Z.: Origin of lower cretaceous ('Nubian')

sandstones of North-east Africa and arabia from detrital zircon U-Pb SHRIMP dating,

Sedimentology, 56(7), 2010–2023, doi:10.1111/j.1365-3091.2009.01067.x, 2009.

445   Kolodny, Y.: The lithostratigraphy and petrology of the Mishash chert Formation, The Hebrew University, Jerusalem., 1965.

Kolodny, Y., Calvo, R. and Rosenfeld, D.: "Too low" δ^{18}O of paleo-meteoric, low latitude, water; do paleo-tropical cyclones explain it?, Palaeogeogr. Palaeoclimatol. Palaeoecol., 280(3–4), 387–395, doi:10.1016/j.palaeo.2009.06.025, 2009.

450   Lal, D.: Cosmic ray labeling of erosion surfaces: in situ nuclide production rates and erosion models, Earth Planet. Sci. Lett., 104(2–4), 424–439, doi:10.1016/0012-821X(91)90220-C, 1991.

Libarkin, J. C., Quade, J., Chase, C. G., Poths, J. and McIntosh, W.: Measurement of ancient cosmogenic ^{21}Ne in quartz from the 28 Ma Fish Canyon Tuff, Colorado, Chem. Geol., 186, 199–213, doi:10.1016/S0009-2541(01)00411-9, 2002.

455   Luna, L. V., Bookhagen, B., Niedermann, S., Rugel, G., Scharf, A. and Merchel, S.: Glacial chronology and production rate cross-calibration of five cosmogenic nuclide and mineral systems from the southern Central Andean Plateau, Earth Planet. Sci. Lett., 500, 242–253, doi:10.1016/j.epsl.2018.07.034, 2018.

Matmon, A. and Zilberman, E.: Landscape Evolution Along the Dead Sea Fault and Its Margins,
460   in Quaternary of the Levant, edited by Y. Enzel and O. Bar-Yosef, p. 771, Cambridge University Press., 2016.

Matmon, A. and Zilberman, E.: Landscape Evolution along the Dead Sea Fault and its Margins, in Quaternary of the Levant, edited by Y. Enzel and O. Bar-Yosef, pp. 17–30, Cambridge University Press., 2017.

465   Matmon, A., Simhai, O., Amit, R., Haviv, I., Porat, N., McDonald, E., Benedetti, L. and Finkel, R.: Desert pavement-coated surfaces in extreme deserts present the longest-lived landforms on Earth, Geol. Soc. Am. Bull., 121(5–6), 688–697, doi:10.1130/B26422.1, 2009.

Meulenkamp, J. E. and Sissingh, W.: Tertiary palaeogeography and tectonostratigraphic evolution of the Northern and Southern Peri-Tethys platforms and the intermediate domains of
470   the African–Eurasian convergent plate boundary zone, Palaeogeogr. Palaeoclimatol. Palaeoecol., 196(1–2), 209–228, doi:10.1016/S0031-0182(03)00319-5, 2003.

Morag, N., Haviv, I., Eyal, M., Kohn, B. P. and Feinstein, S.: Early flank uplift along the Suez Rift: Implications for the role of mantle plumes and the onset of the Dead Sea Transform, Earth Planet. Sci. Lett., 516, 56–65, doi:10.1016/j.epsl.2019.03.002, 2019.

475 Omar, G. I. and Steckler, M. S.: Fission Track Evidence on the Initial Rifting of the Red Sea:
Two Pulses, No Propagation, Science., 270(5240), 1341–1344,
doi:10.1126/science.270.5240.1341, 1995.

Omar, G. I., Steckler, M. S., Buck, W. R. and Kohn, B. P.: Fission-track analysis of basement
apatites at the western margin of the Gulf of Suez rift, Egypt: evidence for synchroneity of uplift
480 and subsidence, Earth Planet. Sci. Lett., 94(3–4), 316–328, doi:10.1016/0012-821X(89)90149-0,
1989.

Romans, B. W., Castelltort, S., Covault, J. A., Fildani, A. and Walsh, J. P.: Environmental signal
propagation in sedimentary systems across timescales, Earth-Science Rev., 153, 7–29,
doi:10.1016/j.earscirev.2015.07.012, 2016.

485 Schaller, M. and Ehlers, T. A.: Limits to quantifying climate driven changes in denudation rates
with cosmogenic radionuclides, Earth Planet. Sci. Lett., 248(1–2), 153–167,
doi:10.1016/j.epsl.2006.05.027, 2006.

Shuster, D. L. and Farley, K. A.: Diffusion kinetics of proton-induced 21Ne, 3He, and 4He in
quartz, Geochim. Cosmochim. Acta, 69(9), 2349–2359, doi:10.1016/j.gca.2004.11.002, 2005.

490 Sinclair, H. D., Stuart, F. M., Mudd, S. M., McCann, L. and Tao, Z.: Detrital cosmogenic 21Ne
records decoupling of source-to-sink signals by sediment storage and recycling in Miocene to
present rivers of the Great Plains, Nebraska, USA, Geology, 47(1), 3–6, doi:10.1130/G45391.1,
2019.

Stone, J. O.: Air pressure and cosmogenic isotope production, J. Geophys. Res. Solid Earth,
495 105(B10), 23753–23759, doi:10.1029/2000JB900181, 2000.

Tchernov, E., Ginsburg, L., Tassy, P. and Goldsmith, N. F.: Miocene mammals of the Negev
(Israel), J. Vertebr. Paleontol., 7(3), 284–310, doi:10.1080/02724634.1987.10011661, 1987.

Val, P., Hoke, G. D., Fosdick, J. C. and Wittmann, H.: Reconciling tectonic shortening,
sedimentation and spatial patterns of erosion from 10Be paleo-erosion rates in the Argentine
500 Precordillera, Earth Planet. Sci. Lett., 450, 173–185, doi:10.1016/j.epsl.2016.06.015, 2016.

Vance, D., Bickle, M., Ivy-Ochs, S. and Kubik, P. W.: Erosion and exhumation in the Himalaya
from cosmogenic isotope inventories of river sediments, Earth Planet. Sci. Lett., 206(3–4), 273–
288, doi:10.1016/S0012-821X(02)01102-0, 2003.

Whipple, K. X.: The influence of climate on the tectonic evolution of mountain belts, Nat.
505 Geosci., 2(2), 97–104, doi:10.1038/ngeo413, 2009.

Whittaker, A. C.: How do landscapes record tectonics and climate?, Lithosphere, 4(2), 160–164, doi:10.1130/RF.L003.1, 2012.

Whybrow, P. J. and McClure, H. A.: Fossil mangrove roots and palaeoenvironments of the miocene of the eastern Arabian Peninsula, Palaeogeogr. Palaeoclimatol. Palaeoecol., 32, 213–225, doi:10.1016/0031-0182(80)90041-3, 1980.

510

Willenbring, J. K., Gasparini, N. M., Crosby, B. T. and Brocard, G.: What does a mean mean? The temporal evolution of detrital cosmogenic denudation rates in a transient landscape, Geology, 41(12), 1215–1218, doi:10.1130/G34746.1, 2013.

Wilson, J. W. P., Roberts, G. G., Hoggard, M. J. and White, N. J.: Cenozoic epeirogeny of the Arabian Peninsula from drainage modeling, Geochemistry, Geophys. Geosystems, 15(10), 3723–3761, doi:10.1002/2014GC005283, 2014.

515

Zilberman, E. and Calvo, R.: Remnants of Miocene fluvial sediments in the Negev Desert, Israel, and the Jordanian Plateau: Evidence for an extensive subsiding basin in the northwestern margins of the Arabian plate, J. African Earth Sci., 82, 33–53, doi:10.1016/j.jafrearsci.2013.02.006, 2013.

520

Earth **Surface**
Dynamics
Discussions

Table 1: Sample Description, Sampling Site Locations and Cosmogenic Nuclide Data

Sample	Sample type	Site	Sampling depth below surface (m)	Location Lat (°N)	Long (°E)	Elevation (m.a.s.l)	Be Carrier (µg)	$^{10}Be/^{9}Be$ (×10⁻¹³)	[^{10}Be] (10⁵ atoms g⁻¹ SiO₂)	$^{26}Al/^{27}Al$	[Al]* (ppm)	[^{26}Al] (10⁵ atoms g⁻¹ SiO₂)	Al/Be	[$^{21}Ne_{cos}$]† (10⁶ atoms g⁻¹ SiO₂)
MHS1	Quartz sand	Paran Valley, Israel	30	30.33296	34.92724	290	178	0.17±0.03	0.14±0.02	NA	104	NA	NA	3.66±1.91
MHS3	Quartz sand	Arad Quarry, Israel	90	31.23372	35.20685	570	176	0.36±0.02	0.29±0.02	0.60±0.08	110	1.33±0.17	4.57±064	8.97±1.39
MHS5	Quartz sand	Arad Quarry, Israel	100	31.23372	35.20685	570	171	0.32±0.02	0.26±0.02	0.35±0.04	114	0.86±0.11	3.25±0.44	8.89±1.83
MHC2	Chert pebble	Paran Valley, Israel	20	30.33296	34.92724	290	NA	NA	NA	NA	NA	NA	NA	0.00±0.00
MHC3	Chert pebble	Arad Quarry, Israel	90	31.23372	35.20685	570	NA	NA	NA	NA	NA	NA	NA	5.33±2.49
MHC5a	Chert pebble	Arad Quarry, Israel	100	31.23372	35.20685	570	NA	NA	NA	NA	NA	NA	NA	2.91±1.72
MHC5b	Chert pebble	Arad Quarry, Israel	100	31.23372	35.20685	570	180	NA	NA	0.93±0.12	203	4.33±0.55	NA	0.00±1.88
MHC6	Chert pebble	Paran Valley, Israel	30	30.33296	34.92724	290	172	0.10±0.01	0.39±0.03	0.05±0.02	287	0.32±0.13	0.83±0.35	3.87±2.24
EJC3	In situ chert	Central Jordanian Plateau	Surface	30.97045	36.64469	910	170	0.70±0.03	1.13±0.05	1.50±0.10	230	6.81±0.43	5.11±0.38	8.08±1.48
EJC5	In situ chert	Central Jordanian Plateau	Surface	30.87181	36.52129	1000	172	18.43±0.30	29.75±0.49	11.47±0.25	235	72.96±1.54	2.45±0.07	12.10±2.43

Note: NA – not available. Samples were either not analyzed, or no result was attained.
*Measurement uncertainties are ~5%.
†Cosmogenic ^{21}Ne is the excess of ^{21}Ne concentrations relative to the atmospheric $^{21}Ne/^{20}Ne$ ratio, calculated for the low-temperature steps (<950°C for chert and <1250°C for quartz).
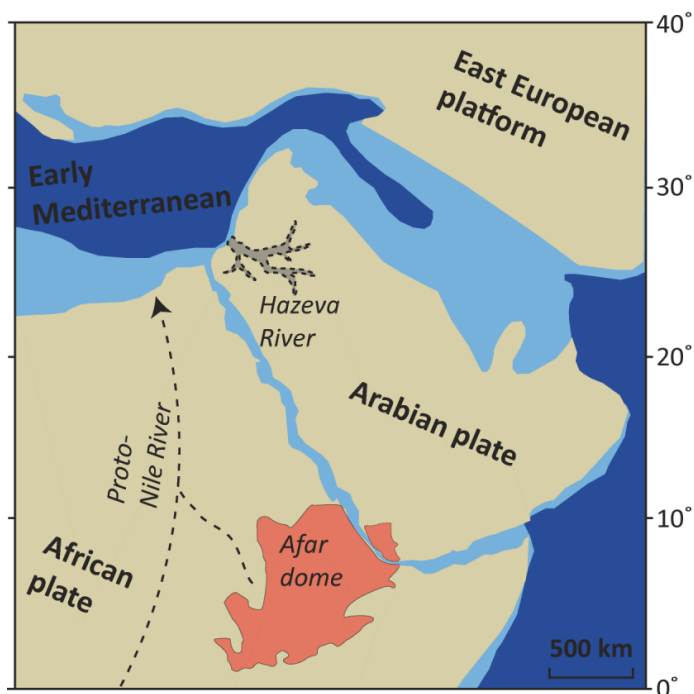
525

Figure 1. Paleo-geographic map of the eastern Levant during the early Miocene (modified after Meulenkamp and Sissingh, 2003) with the approximated extent of the Hazeva fluvial system (based on Avni et al., 2012; Zilberman and Calvo, 2013).

Earth **Surface** Dynamics
Discussions
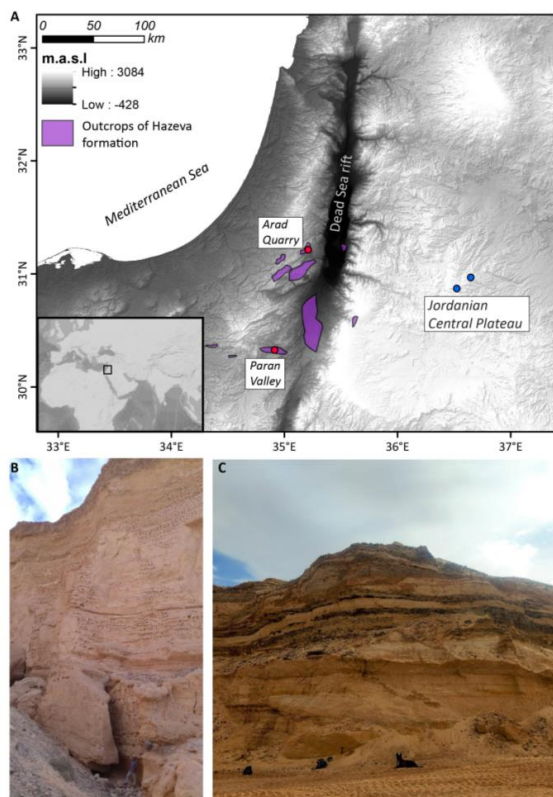
Figure 2. (A) Shaded relief map of the study area with sampling locations of Miocene fluvial sediments sites (red) and in situ Eocene source rock (blue). Hazeva outcrops are after Zilberman and Calvo (2013). Inset map shows regional geographical context. (B) Sampling location at Paran Valley. Sample collected from behind the fallen boulder in a narrow canyon and underneath an overburden of ~50 meters of sand and conglomerate. (C) Photo of sampling location at Arad Quarry. Samples collected from underneath an overburden of ~100 meters of quartz sand.

Earth **Surface**
Dynamics
Discussions
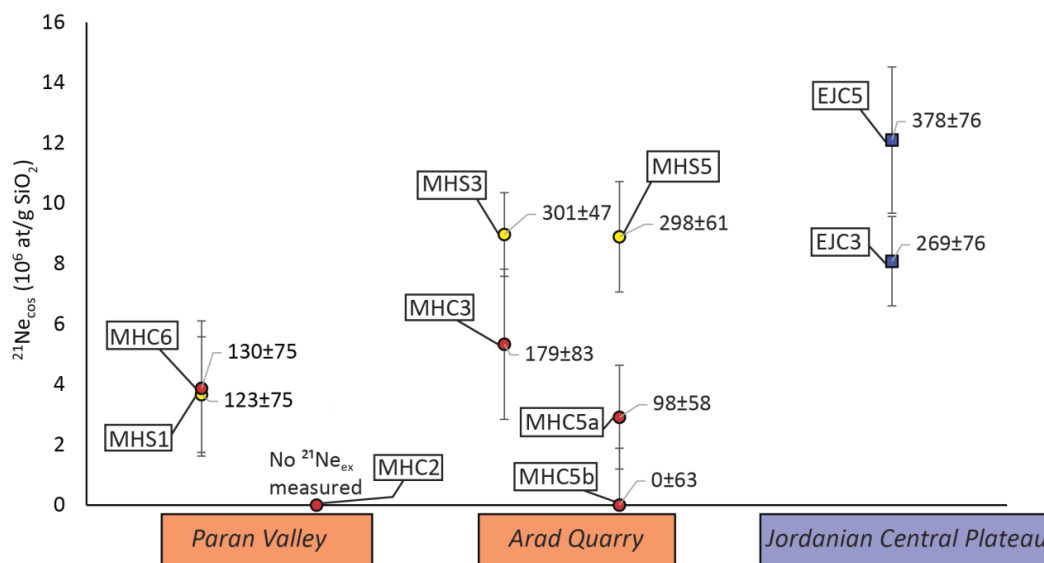
Figure 3. $^{21}Ne_{cos}$ **concentrations in Hazeva sands (yellow), Hazeva chert pebbles (red), and in situ Jordanian Central Plateau chert nodules (blue) with respective uncertainties. Exposure ages, reported in kyr, are calculated using production rates scaled for latitude and altitude after Stone (2000), using ^{21}Ne production rate of 18.1 atoms/g SiO$_2$ year (Borchers et al., 2016; Luna et al., 2018).**

540

Earth **Surface**
Dynamics
Discussions
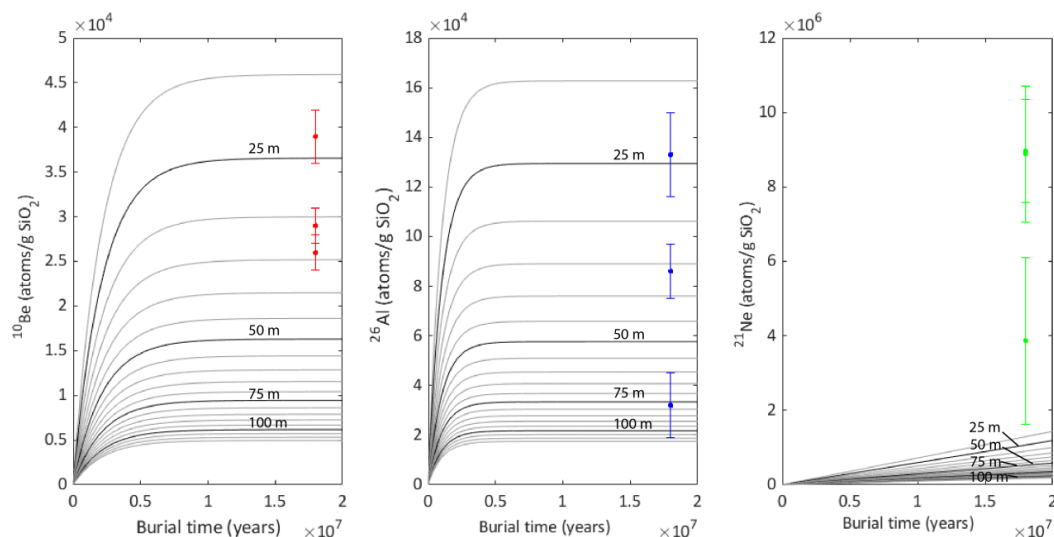
Figure 4. Measured concentrations of ¹⁰Be (red), ²⁶Al (blue), and ²¹Ne (green) in samples MHS3, MHS5, and MHC6. Grey contour lines show changes in nuclide concentrations with time at different depths from 20 to 120 m below the surface in 5m increments. For both sand samples and chert sample, the concentrations of cosmogenic ²¹Ne are higher than the estimated post burial production. Production by cosmic-ray muons is calculated with schematics presented by Balco (2007). Production rates by cosmic-ray muons of ¹⁰Be and ²⁶Al are after Balco (2017) and of ²¹Ne by fast muons is after Balco et al. (2019). This shows that ¹⁰Be and ²⁶Al concentrations can be explained by post-burial production, but ²¹Ne concentrations cannot, so a significant fraction of cosmogenic ²¹Ne is pre-burial.

545

550